Toward Parathyroid Hormone Minimization: Conformational Studies of Cyclic PTH(1−14) Analogues

Natia Tsomaia,[#] Maria Pellegrini,[#,⊥] Kimberly Hyde,[#] Thomas J. Gardella,[§] and Dale F. Mierke*[,‡,#]

Department of Molecular Pharmacology, Division of Biology & Medicine, and Department of Chemistry, Brown University, Providence, Rhode Island 02912, and Endocrine Unit, Massachusetts General Hospital and Harvard Medical School, Boston, Massachusetts 02114

Received September 19, 2003; Revised Manuscript Received November 5, 2003

ABSTRACT: The N-terminal fragment of PTH(1−34) is critical for PTH1 receptor activation. Various modifications of PTH(1−14) have been shown to result in a considerable increase in signaling potency [Shimizu et al. (2000) *J. Biol. Chem. 275*, 21836−21843]. Our structural investigations revealed an unusually stable helical structure of the signaling domain (1−14), where residues 6 (Gln) and 10 (Gln or Asn) were located on the same face of the α-helix. To test whether a stable N-terminal α-helix is required for productive interaction with PTH1 receptor, we designed two conformationally restricted PTH(1−14) analogues, each containing a lactam bridge at positions 6 and 10. Specifically, substitutions $Gln^6 \rightarrow Glu^6$ and $Asn^{10} \rightarrow Lys^{10}$ were introduced into the most potent [$Ala^{1,3,12}$,Gln^{10},Har^{11},Trp^{14}]PTH(1−14)NH_2 agonist. Both the Glu^6−Lys^{10} and Lys^6−Glu^{10} lactam-bridged analogues were characterized to examine the importance of orientation of the lactam. According to biological studies [Shimizu et al. (2003) *Biochemistry 42*, 2282−2290], none of the 6/10 substituted analogues (linear or cyclic) remained as active as the parent peptide. However, relative to their corresponding linear peptides, lactam-bridged analogues either maintained potency or showed 6-fold improvement. High-resolution structures as determined by ^{1}H NMR and NOE-restrained molecular dynamics simulations clearly illustrate the structural differences between the linear and cyclic PTH(1−14) fragments, supporting the hypothesis that an α-helix is the preferred bioactive conformation of the N-terminal fragment of PTH. In addition, our results demonstrate that the structural order of the very first residues (1−4) of the signaling domain plays a significant role in PTH action.

Parathyroid hormone (PTH)[1] plays a critical role in regulating ionized blood calcium levels in the human body (*1*, *2*). The biological actions of PTH (84-amino acid protein) are facilitated through the interaction with the PTH type 1 receptor (PTH1), a member of the class II of G-protein-coupled receptors. Given the potent anabolic effects of PTH on bone density, PTH1 receptor agonists may provide an avenue for the treatment of osteoporosis (*3*, *4*). Consequently, the development of reduced size PTH agonist analogues has been the subject of extensive research (*5*−*12*). It has been explicitly shown that the first 34-amino acid fragment of PTH is sufficient for binding and activating PTH1. Also, numerous studies have suggested that residues 1−9 of PTH(1−34) form a critical receptor activation domain (signaling domain), while residues 15−34 are responsible for binding. However, the complex mechanism of the receptor−ligand interaction and the structure of PTH(1−34) in the receptor-bound state are still unknown.

Recent investigations focusing on the interaction of the signaling portion of PTH with PTH1 (*11*−*14*) showed that certain modifications of N-terminal fragments of PTH can increase signaling potency in peptides as short as 11 amino acids. Specifically, $Ser^3 \rightarrow$ Ala, $Asn^{10} \rightarrow$ Ala or Gln, $Leu^{11} \rightarrow$ Arg, $Gly^{12} \rightarrow$ Ala, and $His^{14} \rightarrow$ Trp, all natural amino acid substitutions, have resulted in enhanced activity of N-terminal PTH fragments in the absence of the PTH(15−34) binding domain (*12*). In certain cases, enhanced potency of the PTH(1−14)NH_2 fragment was achieved by introducing nonnatural amino acids, e.g., a homoarginine at position 11 leading to a 30-fold increase in activity. Furthermore, consistent with molecular models of the ligand/receptor complex (*15*), in vitro studies have detected the functional intolerance of residues Val^2, Ile^5, and Met^8 in the N-terminus of the ligand. The most recent work (*11*) has shown that combining all previously identified activity-enhancing substitutions yields a 1500-fold more potent analogue than the native PTH(1−14)NH_2 fragment ($EC_{50} = 0.12 \pm 0.04$ and 190 ± 20 μM, respectively). However, the detailed mechanism by which the above-mentioned modifications enhance

* To whom correspondence should be addressed: Dale F. Mierke, Department of Molecular Pharmacology, Division of Biology and Medicine, Brown University, Providence RI, 02912. Voice: (401) 863-2139, Fax: (401) 963-1595. E-mail: Dale_Mierke@Brown.edu.

[#] Department of Molecular Pharmacology, Division of Biology & Medicine, Brown University.

[‡] Department of Chemistry, Brown University.

[§] Massachusetts General Hospital and Harvard Medical School.

[⊥] Current Address: Biogen, Inc, 14 Cambridge Center, Cambridge MA, 02142.

[1] Abbreviations: PTH, parathyroid hormone; PTHrP, PTH-related peptide; NMR, nuclear magnetic resonance; CSI, chemical shift index; DG, distance geometry; DPC, dodecylphosphocholine; MD, molecular dynamics; NOE, nuclear Overhauser effect; NOESY, nuclear Overhauser effect spectroscopy; TOCSY, total correlation spectroscopy; RMSD, root-mean-square deviation; CD, circular dichroism; Har, homoarginine; TM, transmembrane; PTH1, parathyroid hormone receptor 1; EC, extracellular loop; ECM, extracellular matrix.

10.1021/bi035703i CCC: $27.50
Published on Web 12/25/2003

Table 1: Amino Acid Sequences and Nomenclature of the Linear and Lactam-Bridged PTH (1−14) Analogues

peptide no.	sequence[a]	lactam position	peptide name[b,c]
1	A−V−A−E−I−E−L−M−H−K−Har−A−K−W−NH_2	none	[M1]PTH(1−14)NH_2
2	A−V−A−E−I−E-L−M−H−K−Har−A−K−W−NH_2	Glu^6−Lys^{10}	cycloEK-[M1]PTH(1−14)NH_2
3	A−V−A−E−I−K-L−M−H−E−Har−A−K−W−NH_2	Lys^6−Glu^{10}	cycloKE-[M2]PTH(1−14)NH_2

[a] Har = homoarginine. [b] M1 = $Ala^{1,3,12}$,Glu^6,Lys^{10},Har^{11},Trp^{14}. [c] M2 = $Ala^{1,3,12}$,Lys^6,Glu^{10},Har^{11},Trp^{14}.

the activity of the truncated PTH analogues is still not known.

To determine the structural basis for the different biological action of modified PTH(1−14) fragments, we began our investigation with one of the potent analogues, [$Ala^{3,10,12}$, Arg^{11}]PTH(1−14). Our NMR analysis in solution of dodecylphosphocholine (DPC) micelles indicated the presence of an α-helix extending through the entire sequence. We postulated that such an unusually stable α-helix extending to the extreme N-terminus stipulated the observed potency of this analogue. To test this hypothesis, we targeted further structural modifications to stabilize the helical structure in the reduced-size N-terminal PTH(1−14) analogues.

One of the well-established strategies to induce or stabilize helical structure in peptides is the introduction of (i, i + 4) spaced Glu−Lys side-chain-to-side-chain lactam bridges (*8*, *16*, *17*). The lactam cyclization stabilizes helical domains and reduces the conformational freedom of linear peptides. Structure−property studies of such sterically restricted, cyclic PTH(1−14) fragments would allow us to validate the relevance of the α-helical domain to the bioactive conformation of PTH-derived agonists. The structural features of [$Ala^{3,10,12}$, Arg^{11}]PTH(1−14) include Glu^6 and Ala^{10} located on the same face of the N-terminal α-helix with their side chains in close proximity to each other, providing the point for introduction of the lactam bridge into the most potent [$Ala^{1,3,12}$,Gln^{10},Har^{11},Trp^{14}]PTH(1−14)NH_2 agonist. Both the Glu^6−Lys^{10} and Lys^6−Glu^{10} are characterized to examine the importance of orientation of the lactam bridge. Here, we report the structural features of the linear analogue [$Ala^{1,3,12}$,Glu^6,Lys^{10},Har^{11},Trp^{14}]PTH(1−14)NH_2 and the two cyclic, lactam containing peptides: cycloEK-[$Ala^{1,3,12}$,Glu^6,Lys^{10},Har^{11},Trp^{14}]PTH(1−14)NH_2 and cycloKE- [$Ala^{1,3,12}$,Lys^6,Glu^{10},Har^{11},Trp^{14}]PTH(1−14)NH_2, as determined by solution state NMR in a zwitterionic membrane mimetic solvent system. Membrane-induced conformations were refined and examined by metric matrix distance geometry (DG) calculations followed by extensive molecular dynamics (MD) simulations incorporating explicit solvent. An enhanced and more complete understanding of the bioactive conformation should provide the insight necessary for the rational optimization of these reduced size, N-terminal PTH analogues.

EXPERIMENTAL METHODS

Peptides. For the peptide synthesis, purification, and biological activity, see ref *18*. The sequences of the linear and cyclic analogues studied here are listed in Table 1.

NMR Experiments. The samples for NMR experiments were made by dissolving the solid peptides in 600 μL of phosphate buffer (10 mM) with 10% D_2O and pH = 5.8 (uncorrected for isotope effect). The peptide concentration was about 1 mM for each analogue. Initially, NMR spectra of the peptides in buffer were collected and then 40 mg of dodecylphosphocholine-d_{38} (Cambridge Isotopes Laboratories) was added to each sample (∼180 mM DPC) for further analysis.

All NMR spectra were collected at 298−308 K on a Bruker Avance spectrometer operating at a magnetic field strength of 14.01 T. The proton resonance frequency at this field strength is 600.132 MHz. The reported chemical shift values for ^1H are expressed in ppm and internally referenced to the ^1H resonance from 3-(trimethylsilyl)tetradeutero sodium propionate (TSP) at 0.0 ppm.

The amino acid spin systems were identified from total correlation spectroscopy (TOCSY) experiments (*19*). A spin lock field of 10 kHz and mixing time of 50 ms were used employing a MLEV-17 pulse sequence (*20*) for Hartman-Hahn coherence transfer. The sequential assignment and proton−proton distances were obtained from nuclear Overhauser effect spectroscopy (NOESY) (*21*, *22*) experiments performed with 150 ms mixing times. In both experiments, the water signal was suppressed using a WATERGATE sequence (*23*).

All two-dimensional spectra were acquired using the time-proportional phase incrementation method (*24*) collecting 640 FIDs of 2048 data points. Spectra were processed using the NMRPipe software (*25*). The time domain data in both dimensions were multiplied by Gaussian or shifted squared sine bell window functions, zero-filled to 2048 × 1024 real points, followed by Fourier transformation. The processed NMR spectra were imported in Sparky (*26*), where peaks were assigned and integrated.

The secondary shift values were calculated relative to reported Hα chemical shifts in random coil conformations and were averaged over three consecutive residues (*27*). In these calculations, the secondary shift for homoarginine (Har) was obtained by subtracting the Hα value of arginine.

Distance Geometry. Integrated cross-peak volumes from NOESY spectra were converted into distances using the isolated two-spin approximation (*28*). During this conversion, cross-peak volumes of the resolved methylene β and/or γ protons of Glu^4, Ile^5, Met^8, and Lys^{13} (1.78 Å) were used for calibration. Adding and subtracting 10% to the experimental distance restrains created a matrix of experimental upper and lower bounds. A pseudoatom correction was applied to the upper bounds of all unresolved methyl and methylene protons (*29*). To obtain the final distance matrix, the experimental restraints matrix was merged with the matrix representing the geometric distance bounds (holonomic constraints). Using the random metrization algorithm (*30*), a hundred molecular structures were generated in a four-dimensional space for each analogue. These structures were optimized initially in four and then in three dimensions using conjugate gradients and distance driven dynamics (*31*, *32*). Structures with NOE violations greater that 0.3 Å were discarded, leaving more than 90 structures fulfilling the experimental interproton distances and the holonomic con-

straints for each peptide studied. Calculations were performed on SGI workstations and Pentium III (Linux-based) processors using home written programs.

MD Simulations. The conformational search using DG produced one family of structures for each analogue. Consequently, for each peptide one representative, low penalty function DG structure was chosen and energy minimized in vacuo with conjugate gradients using the AMBER force field, ignoring charges. The DISCOVER (Molecular Simulations, Inc.) program within the molecular modeling package Insight II was used for minimization. Molecular dynamics simulations were performed with GROMACS (*33*). To model the water−micelle environment, initially a two-phase simulation box ($x = y = z = 60$ Å), containing typically 5332 water and 322 decane molecules, was constructed (*34*−*36*). The peptide structure was then placed at the water/decane interface. Ionizable functional groups at pH = 5.8 were treated as charged species without adding any counterions. All atoms were treated in the GROMOS-87 force field including Lennard-Jones (1.2 nm cutoff), Coulomb (1.2 nm cutoff), and standard bonded (bond stretching, angle bending, improper and proper dihedrals) interactions. The complete system was energy-minimized using steepest descent algorithm. To optimize solvent−peptide interactions, a 10 ps long MD simulation with a 2 fs time step was performed, while the peptide conformation was constrained (force constant 1000 KJ mol^{-1} nm^{-1}). The experimental constraints were then introduced (force constant 2000 KJ mol^{-1} nm^{-1}) and the final MD simulations at 300 K (with 0.02 ps temperature bath coupling) were performed for 500 ps. During the simulation the integration time step was 1 fs, and the applied constant pressure was 1 bar. All simulations were performed on Pentium III processors using GROMACS (*33*).

Molecular Modeling of the Receptor−*Ligand Complex*. Utilizing photoaffinity cross-linking points, homology analysis (theoretical), and structural data of the receptor fragments from NMR spectroscopy and MD simulations, a model of the receptor−ligand complex (PTH1/PTH) for parathyroid hormone has been previously described (*15*). According to this model, the PTH(1−14) ligand "enters" the central part of the PTH1 receptor between the N-terminus/TM1 and TM7 (*37*), and is located in a core formed by seven transmembrane helices of PTH1. For the studies of the PTH(1−14)/PTH1 complex the same model for PTH1 was utilized. The high-resolution NMR structures of the linear and two cyclic PTH-(1−14) analogues reported here were docked into the PTH1 receptor utilizing two ligand/receptor contact points: Val^2−M425 and Lys^{13}−R186 from the photoaffinity cross-linking studies placed within 12 Å (between their alpha-carbons). Each PTH1/PTH(1−14) complex was placed in a three-layer (water/decane/water) simulation cell, to mimic the membrane environment. The seven-helix bundle of the receptor was located in a 45 Å layer of decane molecules, with approximately 40 Å of water molecules above and below. The simulation cell was 12.5 × 12 × 11 Å and consisted of on average 34 000 water molecules and 1210 decane molecules. InsightII (Molecular Simulations Inc.) was used to orient the ligand−receptor complex in the simulation cell. The refinement consisted of three stages. First, the system was energy minimized and equilibrated for 1000 steps (steepest descent algorithm) at 300 K. Second, a short MD (10 ps, 300 K) was performed with position restraints applied to the heavy atoms of the receptor and ligand (force constant 1000 kJ mol^{-1} nm^{-2}) to relax the solvent system relative to the PTH−receptor complex. Finally, the complex was allowed to evolve freely during a 500 ps MD run. During the simulations, the seven TM α-helices of PTH1 were maintained by the appropriate dihedral angle restraints, and the NOE-derived distance restraints were applied to PTH(1−14) ligands. All MD simulations were carried out using periodic boundary conditions. Neighbor lists were updated every 10 steps. Only nonbonded interactions within 8 Å (van der Waals) and 10 Å (Coulomb) were included. A temperature of 300 K was maintained via temperature bath coupling with a time constant of 20 fs. This process was repeated three times for the linear and two cyclic PTH(1−14) ligands, listed in Table 1. All MD simulations were carried out with the GROMACS program (*33*), version 3.1, on a Pentium-based processor running Red Hat Linux 8.0.

RESULTS

NMR Spectroscopy. The secondary shift values, shown in Figure 1(a,b,c), were calculated for all studied peptides (Table 1) in aqueous solution (pH = 5.8) without micelles (gray bars) and in the presence 180 mM DPC lipids (black bars). These plots provide a first estimate of secondary structure. Given that α-helices are identified by negative secondary shift values (*38*), all three samples show some helical content. Furthermore, helices become more pronounced in the presence of DPC micelles for all analogues studied. For the linear [M1]PTH(1−14)NH_2 and cycloKE-[M2]PTH(1−14)NH_2 peptides, analyzed in water solution (Figure 1a,c, gray bars), the secondary shift values are mostly on the order of 0.1 ppm, indicating poorly ordered, conformations. On the contrary, for the lactam-bridged cycloEK-[M1]PTH(*1*−*14*) analogue in the aqueous solution, a well-defined helix is localized between residues Ile^5−Ala^{12}, and the negative deviations become even stronger in the presence of DPC micelles. Interestingly, the secondary shift values (∼0.28) observed for the first few residues (starting from Val^2) of cycloKE-[M2]PTH(1−14)NH_2 in DPC (Figure 1c, black bars) suggest an ordered secondary structure of the N-terminus, while all other secondary shift patterns in Figure 1 are consistent with the absence of stable helix in the N-terminal portions of studied peptides.

The proton NMR spectra of the PTH(1−14) analogues were assigned using standard procedures (*38*). Examples of TOCSY and NOESY spectra in the fingerprint region for two cyclic molecules (cycloEK-[M1]PTH(1−14)NH_2 and cycloKE-[M2]PTH(1−14)NH_2) are shown in Figure 2a,b,c,d. The assignments of the amide protons are displayed only for the TOCSY resonances. For all three peptides studied in DPC, the summary of NOESY connectivities, relevant for determination of their secondary structures, is listed in Figure 3a,b,c. Most of the sequential NH(i)−NH(i + 1) interactions are observed between resolved peaks of lactam-bridged analogues, consistent with generally well-structured conformations. For the linear [M1]PTH(1−14)NH_2 peptide, however, NH(i)−NH(i + 1) cross-peaks are detected starting from Glu.[4] From the NOE pattern [αH(i)−NH(i + 3), αH(i)−βH(i + 3) and αH(i)−NH(i + 4) resonances], α-helical segments can be identified from Ala^3 to Lys^{13} for cycloEK-[M1]PTH(1−14)NH_2 (Figure 3b), and from Ala^1

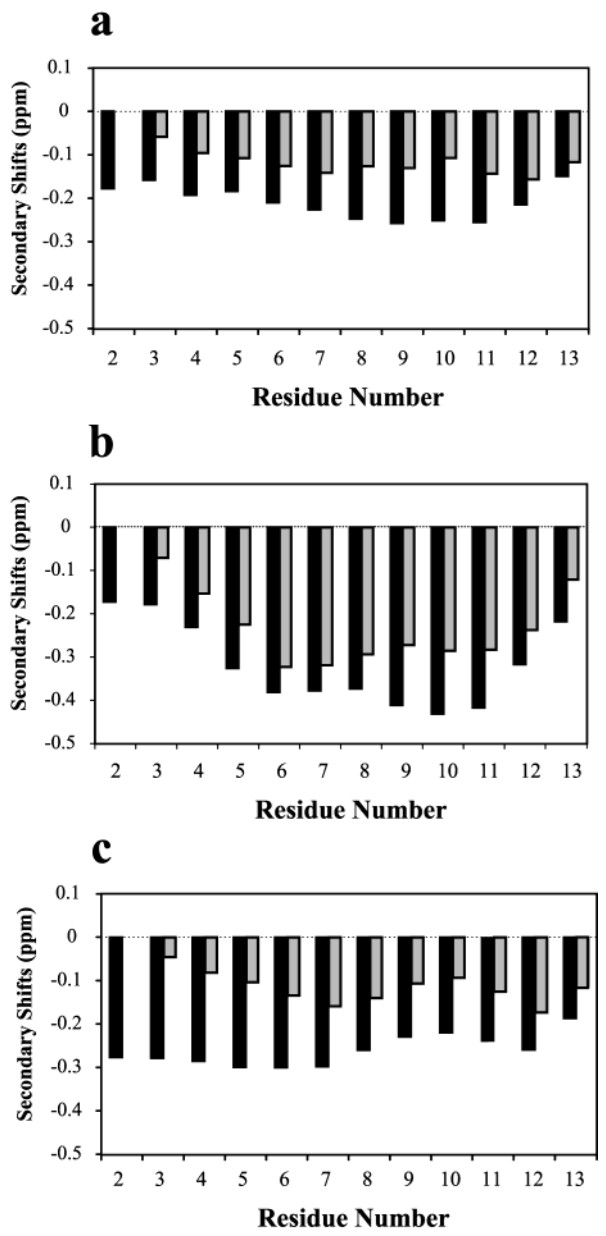

FIGURE 1: Chemical shift differences of the Cα protons relative to their random coil values of (a) [M1]PTH(1−14)NH_2 analogue, (b) cycloEK-[M1]PTH(1−14)NH_2 analogue, and (c) cycloKE-[M2]PTH(1−14)NH_2 analogue in aqueous solution (pH = 5.8) without micelles (gray bars) and in the presence of 180 mM DPC lipids (black bars).

to Ala^{12} for cycloKE-[M2]PTH(1−14)NH_2 (Figure 3c). For the linear analogue (Figure 3a), αH(i)−βH(i + 3) and αH(i)−NH(i + 3) type NOEs are observed from Ile^5 to Trp^{14} region, also including a single αH(i)−NH(i + 4) type cross-peak [αH(5)−NH(9)] (a number of i−(i + 4) NOEs might be overlapped in the NOESY spectrum). No medium-range NOEs are observed in the Ala^1−Glu^4 region of the [M1]-PTH(1−14)NH_2 linear peptide, suggesting disordered conformation for the N-terminus.

Distance Geometry Calculations. From the integration of the NOESY spectrum of linear [M1]PTH(1−14)NH_2 analogue, out of 153 total NOEs, 132 conformationally informative constraints were obtained (13 medium range and 32 sequential). The DG calculations generated 94 structures fulfilling the experimental NMR data; no violations exceeded 0.3 Å for individual conformations. Thirty calculated DG structures (Figure 4) were superimposed in the Glu^6−Lys^{10} region (RMSD 0.9 Å). The backbone dihedral angle order parameter values (*39*), characterizing the conformational distribution, are shown in Figure 5. Calculated structures (Figure 4a) and the order parameters for the linear [M1]PTH-(1−14)NH_2 analogue (Figure 5a) illustrate a well-defined helix in the Ile^5−Lys^{13} region (order parameter > 0.9), relatively flexible C-terminal residues (Trp^{14}, $NH_2{}^{15}$), and mainly extended N-terminus.

For the lactam-bridged cycloEK-[M1]PTH(1−14)NH_2 analogue, out of 171 total NOEs, 133 informative NOE constraints (18 medium range and 31 sequential) were obtained from the NOESY experiment. The conformational search using DG produced 94 structures (out of 100 runs) fulfilling these experimental constraints (with individual violations < 0.3 Å). The convergence (RMSD 0.8 Å for Glu^6−Lys^{10} region) is illustrated in Figure 4b (for clarity, the lactam bridge is displayed for only one representative conformation). Consistent with the observed secondary shift pattern of the cycloEK-[M1]PTH(1−14)NH_2 analogue (Figure 1b), the calculated structures (Figure 4b) and the backbone dihedral angle order parameter values (Figure 5b) indicate a well-defined, stable helical segment extended from Ala^3 to Lys^{13} (order parameter > 0.9).

The NOESY spectrum of cycloKE-[M2]PTH(1−14)NH_2 analogue provided 172 NOEs, 146 of which were informative (14 medium range and 35 sequential). DG calculations were repeated 96 times, producing 80 structures fulfilling experimental NOE data (with violations < 0.3 Å). More than 30 superimposed DG conformations (RMSD 1.2 Å for Lys^6−Glu^{10} region), with one representative lactam bridge, are shown in Figure 4c. For this cyclic peptide, the dihedral angle order parameter (Figure 5c) is not as uniform as for cycloEK-[M1]PTH(1−14)NH_2 analogue. The Lys^6−Har^{11} part of the cycloKE-[M2]PTH(1−14)NH_2 is characterized by high order parameter values (>0.88), suggesting that all structures converge to a well-defined helix in the lactam-bridged portion of the peptide. However, strong dispersion of ϕ dihedral angles is observed for residues Ile^5 and Lys^{13} (order parameter < 0.5, Figure 5c), indicating the presence of flexible regions around these positions. Finally, unlike other studied peptides, this cyclic analogue displays relatively high order parameter values (>0.7) for the Val^2−Glu^4 segment. This result is consistent with the secondary shift observations (Figure 1c, black bars) suggesting an ordered conformation extending to the very N-terminus of the cycloKE-[M2]PTH-(1−14)NH_2 peptide.

Molecular Dynamics Simulations. MD simulations using a two-phase (aqueous/hydrophobic) simulation cell, mimicking the membrane environment, were performed to further refine the peptide structures. At the end of 500 ps MD runs the topological orientations adopted by three PTH(1−14) analogues studied are shown in Figures 6−8. Even though the amphiphilic character is not well pronounced for the signaling part (1−14) of PTH, the linear analogue, [M1]PTH(1−14)NH_2, has its charged residues Glu^6 and Lys^{10} directed toward the water phase, while hydrophobic Ile^5 and Met^8 side chains face into the decane layer (Figure 6). Moreover, this peptide adopts α-helical conformation only beyond the residue Ile^5, which is preceded by a 3_{10} helical turn and the extended N-terminal tail. In contrast, the two

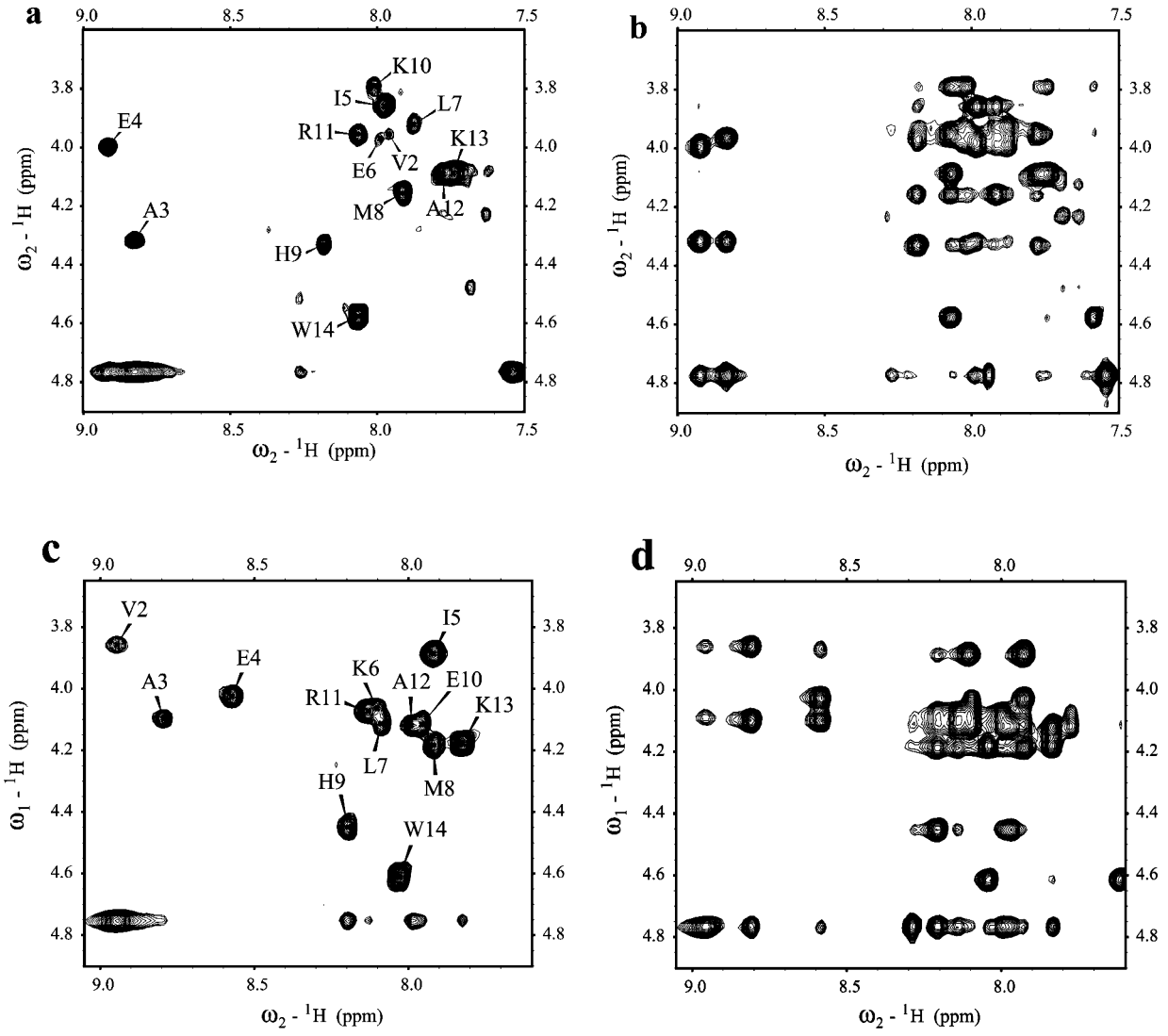

FIGURE 2: Fingerprint regions of the TOCSY (a, c) and NOESY (b, d) spectra of cycloEK-[M1]PTH(1−14)NH_2 (a, b) and cycloKE-[M2]PTH(1−14)NH_2 (c, d) peptides in aqueous solution (pH = 5.8) in the presence on DPC micelles. The assignments are shown only for TOCSY resonances in the amide region.

cyclic analogues converge to well-defined α-helices starting from residue 1, directing the lactam bridges toward the water phase (Figures 7 and 8).

Molecular Modeling of the Receptor−Ligand Complexes. The topological orientation of the linear ligand and the major binding interactions with PTH1 receptor are shown in Figure 9a. The second residue of this analogue, *Val*^{2}, is accommodated in a hydrophobic pocket, mainly defined in the EC2 region of the PTH1 receptor. Measurements indicate that there are 10 amino acids in the PTH1 receptor that have side chain atoms within 6 Å from the two *Val*^{2} γ carbons. The strongest contributors for *Val*^{2} binding pocket (<3.5 Å) include V340, A344, W361, and T427 of the receptor. Residues V340 and A344 belong to the extracellular (EC) region of TM 4, W361 is located on the EC side of TM5 (Figure 9a), and T427 is found on the EC end TM6 (not shown). Additional stabilizing contributions to the same binding site are provided by S341, R343, S356, G357, N358, and V365.

Within this model there are seven amino acids in close spatial proximity (<6 Å) from the γ and δ carbons of *Ile*^{5}. The residues V340, S341, R282, V285, and T427 contribute to this binding cleft with L289 and A344 complement the binding pocket from the TM3 and N-terminal end of EC2, respectively.

The PTH1 receptor accommodates *Met*^{8} in a hydrophobic pocket consisting of V423 (the extracellular end of TM6), F447, N448, and Q451 (EC3 region of TM7) strongly interacting amino acids. Residues V419, S449, and F450 further stabilize the binding site.

Both the *Glu*^{6} and *Lys*^{10} side chains face toward the hydrophilic ECM. The *Glu*^{6} displays strong interactions with R282, A344, T345, and D353 (shown with light green sticks, in Figure 9a), while only L354 and Y245 are in close proximity to *Lys*^{10}, with the positively charged side chain solvent exposed.

The cycloEK-[M1]PTH(1−14)NH_2/PTH1 Complex. Four residues, A344, L354, S355, and W361, are located in the EC2 region of PTH1 receptor, and play a crucial role in the binding of *Val*^{2} of the ligand (Figure 9b). Residue W361 is the closest neighbor, with a distance of 2.36 Å between *Val*^{2} side chain and one of its hydrogen atoms. Other amino acids, with a relatively weak contribution to this binding pocket

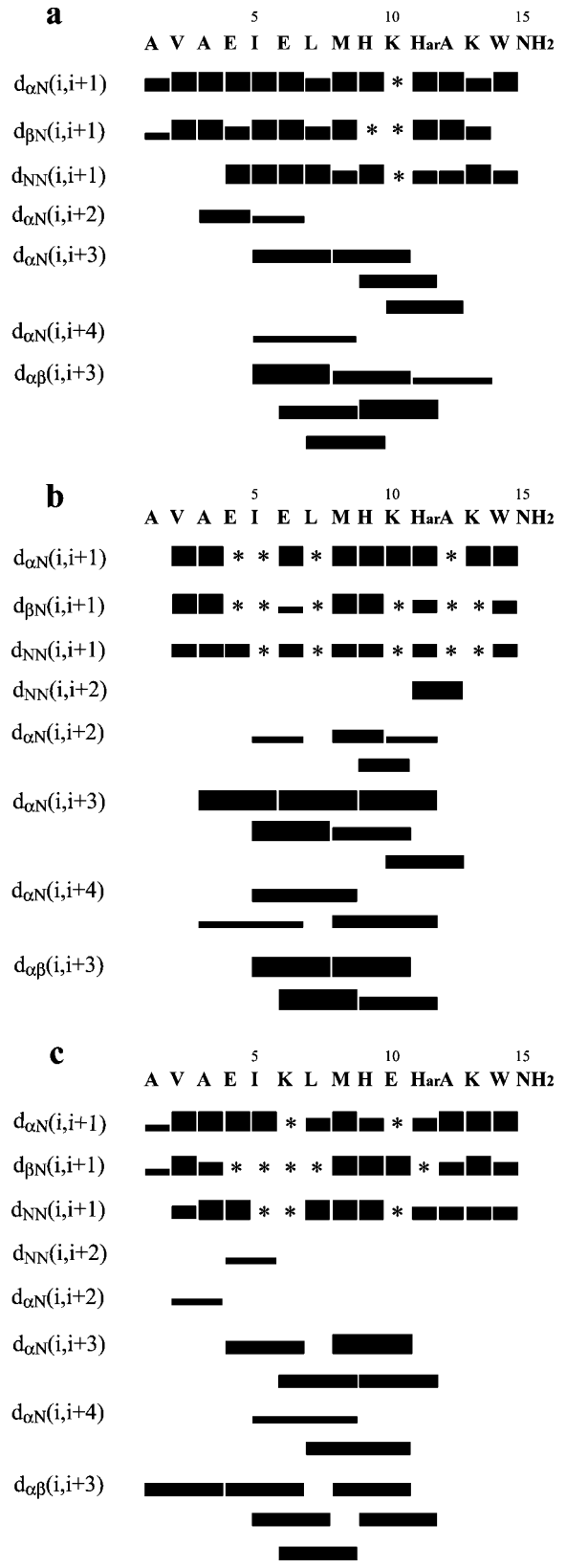

FIGURE 3: Summary of NOESY connectivities of (a) [M1]PTH-(1−14)NH_2 analogue, (b) cycloEK-[M1]PTH(1−14)NH_2 analogue, and (c) cycloKE-[M2]PTH(1−14)NH_2 analogue in water containing 180 mM DPC micelles at pH = 5.8. Peaks are grouped in three classes (strong, medium, and weak) based on their integrated volumes. An asterisk indicates a cross-peak, which could not be identified due to resonance overlap.

include S356 and I362, also located in the EC2 region of the PTH1.

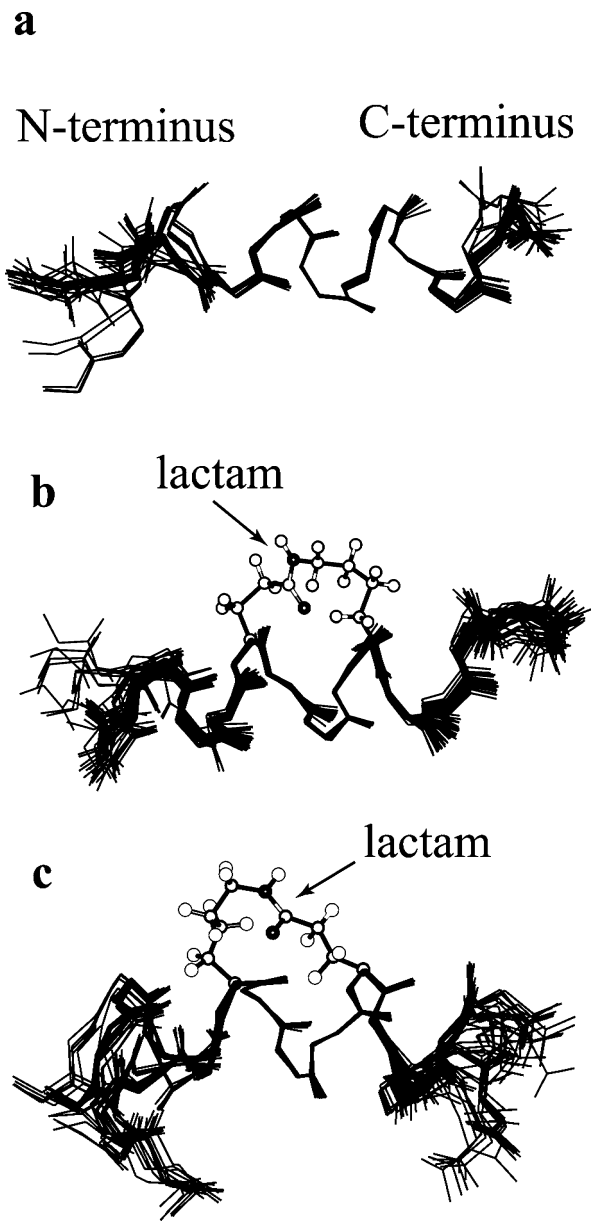

FIGURE 4: Superposition of 30 structures obtained from DG calculations for (a) [M1]PTH(1−14)NH_2 analogue (RMSD 0.9 Å for the Glu^6−Lys^{10} region), (b) cycloEK-[M1]PTH(1−14)NH_2 analogue (RMSD 0.8 Å for the Glu^6−Lys^{10} region), and (c) cycloKE-[M2]PTH(1−14)NH_2 (RMSD 1.2 Å for the Lys^6−Glu^{10} region). For cyclic peptides (b, c) lactam bridge in ball-and-stick representation is shown for a single conformation.

Three receptor residues V285, L354, and F447 show strong interactions with the *Ile*^{5} side chain. According to our model, residue V285 is located in the EC region of TM3, L354 belongs to the EC2, and F447 is positioned in the EC portion of TM7. The V285 is the closest neighbor, containing a hydrogen atom 2.56 Å away from the side chain of *Ile*^{5}. Other contributing interactions include V340, S341 (from EC regions of TM2), and T427 (from EC regions of TM6).

Five amino acids define the hydrophobic pocket of *Met*^{8}. Three residues, with the strongest contribution include V285, F288 (both located on the EC region of TM3), and Q451 (located on the EC region of TM7) with the side chains of F447 and K240 adding to the binding site. The lactam bond between *Glu*^{6} and *Lys*^{10} faces away from the receptor toward the hydrophilic ECM and interacts with residues Y245, W352, D353, L354, and S355.

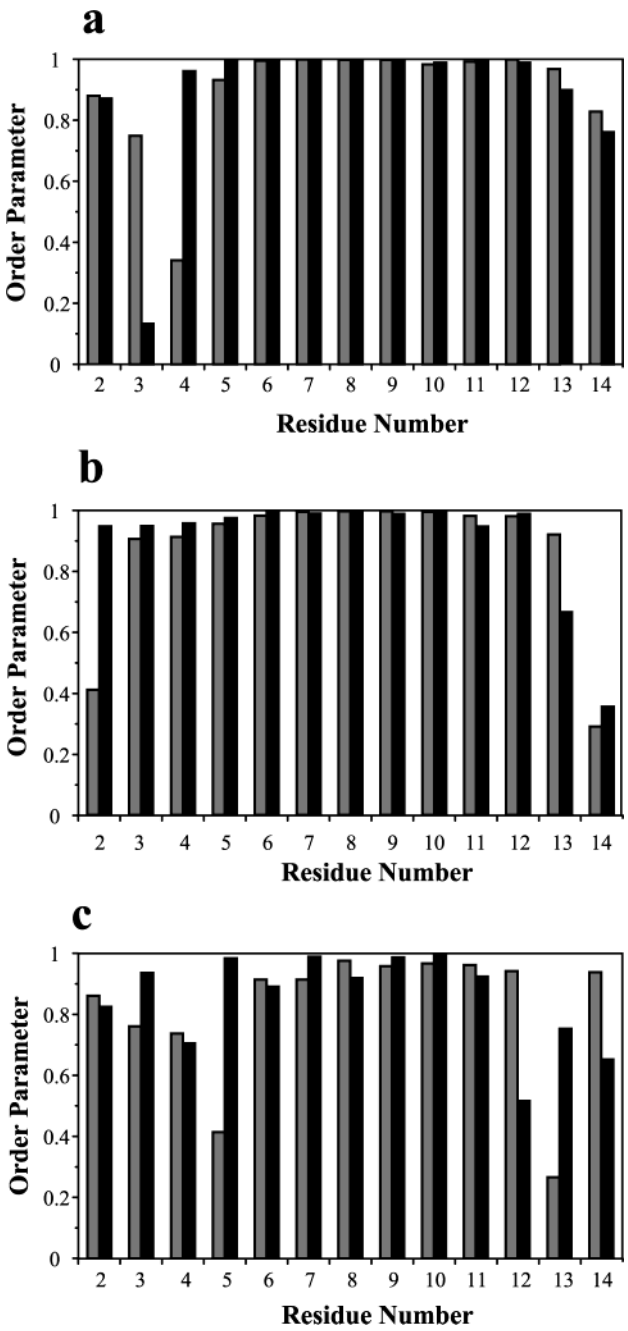

FIGURE 5: Order parameter values for Φ (gray bars) and Ψ (black bars) backbone dihedral angles calculated for the ensembles of structures, obtained from the DG calculations, for (a) [M1]PTH(1−14)NH_2 analogue, (b) cycloEK-[M1]PTH(1−14)NH_2 analogue, and (c) cycloKE-[M2]PTH(1−14)NH_2 analogue.

The cycloKE-[M2]PTH(1−14)NH_2/PTH1 Complex. MD simulation results show that there are only two amino acids, L354 and W361, in the PTH1 strongly interacting with the *Val*^{2} side chain (Figure 9c). Both of these amino acids are located in the EC2 loop, the extracellular region of PTH1 between TM helices 4 and 5.

The strongest interaction from *Ile*^{5} was detected with T427, W361, and F447 residues. In our model, T427 and F447 are located in the EC3 portion of PTH1, extracellular part between TM6 and TM7, while W361 belongs to the N-terminal part of TM5.

Residue *Met*^{8} interacts with four amino acids, T427, E444, M445, and F447, in the PTH1 receptor; they form a nice hydrophobic pocket near the extracellular portion of TM7. The strongest interaction is observed between *Met*^{8} and F447.

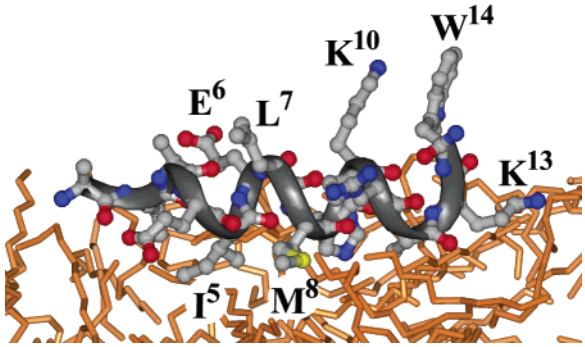

FIGURE 6: The final conformation of linear [M1]PTH(1−14)NH_2 analogue obtained from an NOE-restrained MD simulation (500 ps) in a water−decane membrane mimetic solvent box with periodic boundary conditions. The water phase is not shown for simplicity. The decane phase is depicted in golden-brown sticks. The receptor fragment is shown with dark gray ribbon with the N-terminus oriented to the left; atoms for the receptor amino acids are color coded (red = oxygen, blue = nitrogen, yellow = sulfur, and light gray = carbon).

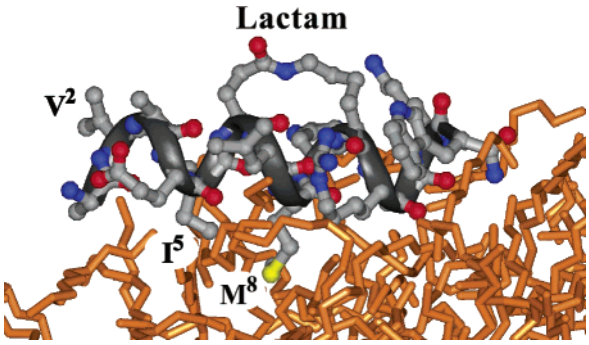

FIGURE 7: The final conformation of cycloEK-[M1]PTH(1−14)NH_2 analogue obtained from 500 ps NOE-restrained MD simulation. The decane phase is depicted in golden-brown CPK. Details are given in Figure 6 caption.

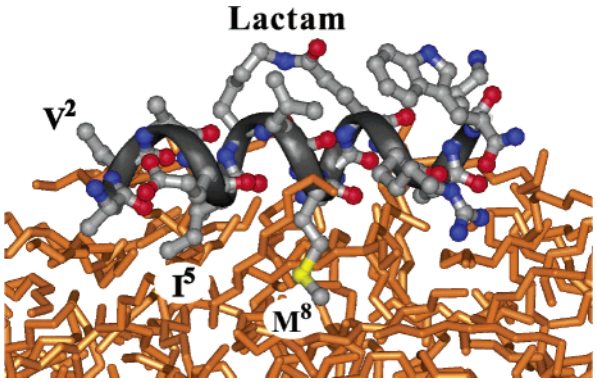

FIGURE 8: The final conformation of cycloKE-[M2]PTH(1−14)NH_2 analogue obtained from 500 ps NOE-restrained MD simulation (see Figure 6 for details).

The lactam bridge between *Lys*^{6} and *Glu*^{10} faces toward the hydrophobic region of the ECM. Amino acids in PTH1 that neighbor lactam (withing 6 Å) include Y245 and W352, from N-terminal part of EC1 and the mid region of EC2 loops, respectively.

DISCUSSION

To stabilize the helical structure, putatively linked to bioactivity of PTH(1−14), Glu^{10}/Lys^6 or Lys^6/Glu^{10} substitu-

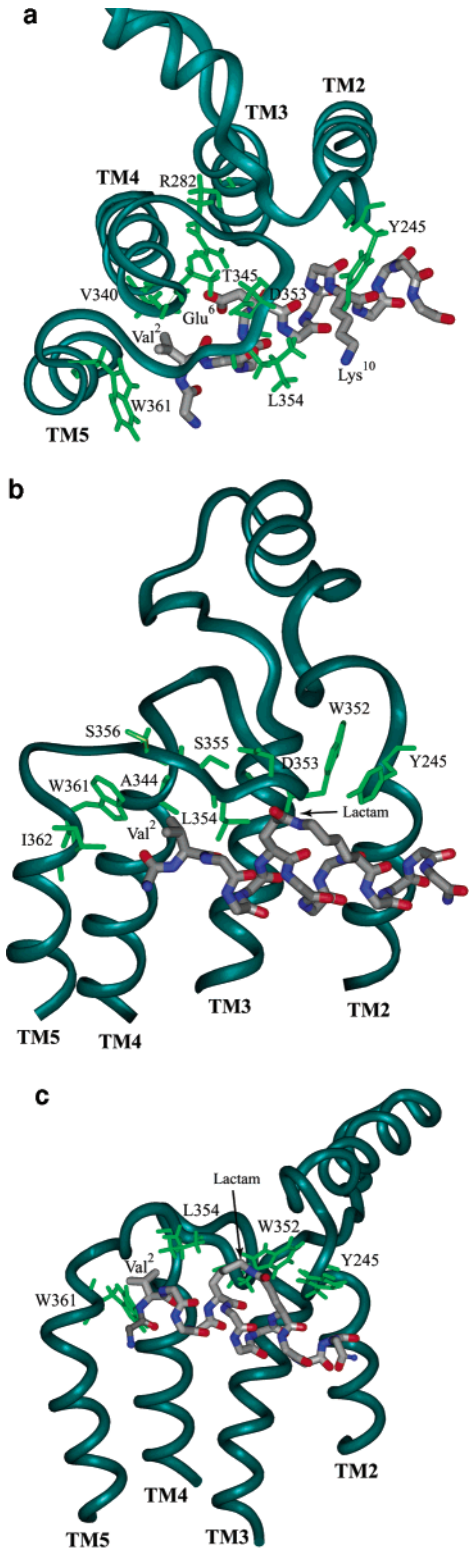

FIGURE 9: Illustration of some of the interactions between PTH(1−14) analogues studied and PTH1 receptor. The receptor cross-section is taken for better view; only TM2-EC1-TM3 and TM4-EC2-TM5 portions of PTH1 are displayed in dark green-blue ribbon. Few receptor side chains, interacting with the ligands, are shown in light green sticks and denoted in the one-letter code. The backbones of the ligands are shown in gray sticks and are color-coded (red = oxygen, blue = nitrogen, and light gray = carbon). For clarity, only Val^2, Glu^6, and Lys^{10} (or Lys^{10}/Glu^6) side chains are displayed for (a) linear [M1]PTH(1−14)NH_2, (b) cycloEK-[M1]-PTH(1−14)NH_2, and (c) cycloKE-[M2]PTH(1−14)NH_2 analogues. The residues of the ligand are shown in the three-letter code.

tions were introduced in the most potent [$Ala^{1,3,12}$,Gln^{10},Har^{11}, Trp^{14}]PTH(1−14)NH_2 analogue. It was anticipated that the cyclization at positions 6 and 10 would produce conformationally constrained PTH agonists, presumably with increased affinities. According to in vitro studies (*18*), however, none of the 6/10 substituted (linear or lactam-bridged) peptides remained as active as the parent compound. Yet, relative to their corresponding linear peptides, lactam-bridged Glu^{10}/Lys^6 and Lys^6/Glu^{10} analogues either maintained potency (cycloEK-[M1]PTH(1−14)NH_2), or demonstrated a 6-fold improvement (cycloKE-[M2]PTH(1−14)NH_2) in signaling. From these results, it is evident that the observed loss of potency in these modified PTH(1−14) fragments does not follow from the lactam cyclization and consequent stabilization of α-helical structure; rather, it is due to the absence of the native Gln^6 residue, which may play a unique role in PTH(1−14) function (*18*). Hence, in favor of our design principle, we found that the conformationally constrained helix is able not only to preserve the determinant interactions of the linear peptide, but also to contribute to the increased biological activity of the modified PTH(1−14) fragment. Indeed, we cannot rule out that the source of the enhanced biological function of the 6/10 cyclization is elimination of unfavorable interactions of the charged Lys side chain. Nonetheless, our in vitro and NMR results suggest that α-helix is a biologically compatible conformation for the signaling (N-terminal) portion of PTH.

A number of prior studies have provided evidence that supports a membrane-bound pathway for the ligand−receptor interaction (*40*−*44*). According to this model, the ligand initially binds to the cell membrane, followed by diffusion on the membrane surface that leads to specific ligand−receptor interaction. The preorganized, cell membrane-associated state of the ligand is believed to resemble its bioactive conformation. Here, we have used DPC micelles as an NMR compatible, zwitterionic membrane mimetic, in our study of the structures of linear ([M1]PTH(1−14)NH_2) and lactam-bridged (cycloEK-[M1]PTH(1−14)NH_2 and cycloKE-[M2]PTH(1−14)NH_2) PTH analogues. The observed secondary shift patterns (Figure 1a,b,c) indicate that two of the peptides studied (Figure 1a,c) dramatically change conformations from extended structures (in water) to well-defined helices (in DPC) upon association with the micelles.

Comparison of the secondary shift values of the linear [M1]PTH(1−14)NH_2 (Figure 1a, gray) and the corresponding cyclic (cycloEK-[M1]PTH(1−14)NH_2) analogues in water (Figure 1b, gray) clearly illustrates the constraining and stabilizing effect of the Glu^6−Lys^{10} lactam bridge. As predicted, due to cyclization of the side chains in positions 6 and 10, this peptide adopts a well-defined α-helical structure, extended between residues Ile^5−Ala^{12}, even in buffered aqueous solution. However, the same is not true for the cycloKE-[M2]PTH(1−14)NH_2 analogue, where the order of the lactam is reversed; despite cyclization, the Lys^6−Glu^{10} bridged fragment preserves its random conformation in water. This outcome is in agreement with previous studies on model peptides documenting that, while the Glu(i)−Lys(i + 4) arrangement in lactam greatly increases the helicity over the corresponding linear peptide, the Lys(i)−Glu(i + 4) bridged analogue is typically less helical (*17*). This orientation effect was attributed to a steric clash of the lactam bridge carbonyl group with the backbone carbonyl. Interest-

ingly, according to the secondary shift pattern, the destabilizing interaction of Lys^6-Glu^{10} bridge disappears in the presence of DPC micelles, and the micelle-bound conformation of cycloKE-[M2]PTH(1−14)NH_2 analogue becomes completely helical starting from residue Val^2. In fact, among all peptides studied here, the DPC-associated Lys^6-Glu^{10} bridged analogue is the only one that displays a highly ordered conformation of its N-terminal portion (Val^2-Ile^5). This result is in accord with structure calculations based on our NOE data. As the observed NOE pattern indicates (Figure 3), the first four residues of the linear analogue are mainly unstructured (Figure 3a), but for cycloKE-[M2]PTH(1−14)-NH_2 peptide helical NOEs are detected stating from Ala^1 (Figure 3c). Note that, among three PTH(1−14) fragments investigated, despite small differences in potency, the linear peptide displays the weakest biological activity, and the Lys^6-Glu^{10} cyclic analogue is the most potent; thus, it is reasonable to search for the correlation between enhanced biological activity and ordered (helical) N-terminus (Ala^1-Glu^4) of these peptides. Interestingly, the same correlation was observed by Shimizu et al. upon substitution of Ala^1 and Ala^3 with the conformationally constraining amino acid, α-aminoisobutyric acid (Aib), in linear [$Ala^{1,3,12}$,Gln^{10},Har^{11}, Trp^{14}]PTH(1−14)NH_2 analogue (*14*). It was shown, that as Aib substitutions at positions 1 and 3 increased helicity (determined by CD spectroscopy), [$Aib^{1,3}$,Gln^{10},Har^{11},Ala^{12},Trp^{14}]PTH(1−14)NH_2 analogue became about 100-fold more potent ($EC_{50} = 1.1 \pm 0.1$ nM) than [$Ala^{1,3,12}$,Gln^{10},Har^{11},Trp^{14}]PTH(1−14)NH_2 peptide ($EC_{50} = 100 \pm 20$ nM), and nearly 100 000-fold more potent than native PTH (1−14). All of these results further the hypothesis of an α-helix as the preferred bioactive conformation of the N-terminus of PTH. Moreover, it appears that the structural order of the very first residues (Ala^1-Glu^4) of the signaling portion (1−14) of PTH plays a significant role in the potency of the peptide.

To gain a better understanding of the molecular mechanism by which the observed functional effects arise in PTH(1−14) analogues, a direct assessment of the structure that the PTH signaling domain adopts in the receptor-bound state is necessary. The molecular dynamics simulations of PTH1/PTH(1−14) receptor−ligand complexes, reported here, provide a detailed structural insight into the biological data described elsewhere (*18*, *45*).

The results of the simulations indicate that the binding mode of linear and cyclic PTH(1−14) analogues, studied here, is consistent with the existing PTH/PTH1 model. Specifically, a well-defined N-terminal helix of PTH is projected toward the seven transmembrane helical bundle of the receptor leading to specific interactions between the N-terminal helix and the extracellular loops. Consistent with the photoaffinity cross-linking data, the second residue (Val^2) remains in close spatial proximity to the EC3 loop in all three ligands studied, and residue 13 (Lys^{13}) resides within 12 Å from the extracellular part of TM1. Note that the side chains of M425 and R186 are projecting away from their photoaffinity cross-linking contact points in the ligand and the seven TM bundle of the receptor. This divergence was expected, considering the difference in the size and the hydrophobic nature of the *para*-benzoylphenylalanine (Bpa) used in the cross-linking experiments and the corresponding natural amino acids in PTH, Val^2 and Lys^{13}.

The positively charged, N-terminal amine groups of α-helical [M1]PTH(1−14)NH_2, cycloEK-[M1]PTH(1−14)-NH_2, and cycloKE-[M2]PTH(1−14)NH_2 analogues are hydrogen bonded to the backbone carbonyl groups (A426, T427, and P428, respectively) at the end of TM6 helix. Given the negative dipole found at the C-terminus of an α-helix, these interactions contribute to the stabilization of the TM6 macrodipole.

The binding pocket of Val^2 for the linear [M1]PTH(1−14)NH_2 analogue is well defined by the hydrophobic residues from the N-terminal portion of TM4 (V340), TM5 (W361), EC2 (A344), and EC3 (T427) loops. This binding cleft, consistent with previous findings (*15*), appears to be shielding the residue 2 of PTH(1−14) from the aqueous environment; Val^2 side chain is directed toward the core, between TM4 and TM5, while EC2 folds over the ligand from the top, and the beginning of EC3 interacts from the side. Most of these van der Waals interactions are depicted in Figure 9a; the EC3 is not shown for simplicity. Note that this binding site slightly differs from the one reported by Rölz et al., where the hydrophobic pocket of Val^2 is mainly created by EC3 loop, and in particular, by residues W437 and Q440. Similarly, for the cyclic analogues, no significant interactions have been observed between Val^2 and EC3; the hydrophobic clefts of Val^2 for the lactam-bridged peptides are defined residues from TM4, TM5, and EC2, as shown in Figure 9b,c. According to previous mutation studies, substitution of W437 and Q440 resulted in a loss of binding affinity for PTH, indicating a dominant role of the EC3 loop in receptor bonding and selectivity. In our model, the absence of strong interactions with the EC3 loop might account for the weak potency of all studied PTH(1−14) analogues, as compared to the native ligand.

In all three complexes studied, the hydrophobic side chains of Ile^5 and Met^8 are directed into the central core of the receptor. The residues Glu^6 and Lys^{10}, located on the same face of the α-helix, project away from TM bundle toward the hydrophilic ECM. Recent biological and structural data on PTH analogues suggest that strong interaction (or hydrogen bond) between side chains 6 and 10 not only stabilizes the helix, but also constrains the position of residue 10 to avoid any unfavorable contacts between the side chain 10 and the receptor. Consistent with these observations, the $Gln^6 \rightarrow Glu^6$ and $Asn^{10} \rightarrow Lys^{10}$ substitutions diminish the signaling potency of the linear analogue, [M1]PTH(1−14)-NH_2, while the potency increases upon the 6/10 lactam cyclization. Our model accounts for these changes; in the linear peptide, [M1]PTH(1−14)NH_2, the Glu^6 side chain is accommodated in a binding cavity created by residue R282 (beginning of TM3) from the bottom, and complemented by the EC2 loop (i.e., T345, D353, and A344) from the top (Figure 9a). Such a topology provides a strong Coulombic interaction between Glu^6 and positively charged R282 of TM3. The Lys^{10} side chain, however, faces away from the receptor core and is exposed to the aqueous environment on the extracellular surface weakly interacting (∼7.7 Å) with C-terminal end of TM7 (i.e., E444). No strong interaction has been detected between the side chains of Glu^6 and Lys^{10}. On the contrary, the lactam bridge of the cyclic peptides is accommodated in a hydrophobic binding pocket that provides strong van der Waals contacts with the EC2 loop (i.e., W352, S355, L354) and the beginning of TM2 (i.e., Y245).

REFERENCES

1. Kronenberg, H. M., Bringhurst, F. R., Nussbaum, S. R., Jüppner, H., Abou-Samra, A. B., Segre, G. V., and Potts, J. T., Jr. (1993) *Handbook of Experimental Pharmacology*, Springer-Verlag, Heidelberg.
2. Broadus, A. E., and Stewart, A. F. (1994) *The Parathyroids: Basic and Clinical Concepts*, Raven Press, New York.
3. Whitfield, J. F., Morley, P., and Willick, G. E. (2000) *Medscape Women's Health 5*, E5.
4. Dempster, D. W., Cosman, F., Parisien, M., Shen, V., and Lindsay, R. (1993) *Endocr. Rev. 14*, 690−709.
5. Maretto, S., Mammi, S., Bissacco, E., Peggion, E., Bisello, A., Rosenblatt, M., Chorev, M., and Mierke, D. F. (1997) *Biochemistry 36*, 3300−3307.
6. Jin, L., Briggs, S. L., Chandrasekhar, S., Chirgadze, N. Y., Clawson, D. K., Schevitz, R. W., Smiley, D. L., Tashjian, A. H., and Zhang, F. (2000) *J. Biol. Chem. 275*, 27238−27244.
7. Marx, U. C., Adermann, K., Bayer, P., Forssmann, W. G., and Rosch, P. (2000) *Biochem. Biophys. Res. Commun. 267*, 213−220.
8. Mierke, D. F., Maretto, S., Schievano, E., DeLuca, D., Bisello, A., Mammi, S., Rosenblatt, M., Peggion, E., and Chorev, M. (1997) *Biochemistry 36*, 10372−10383.
9. Schievano, E., Mammi, S., Bisello, A., Rosenblatt, M., Chorev, M., and Peggion, E. (1999) *J. Pept. Sci. 5*, 330−337.
10. Pellegrini, M., Royo, M., Rosenblatt, M., Chorev, M., and Mierke, D. F. (1998) *J. Biol. Chem. 273*, 10420−10427.
11. Shimizu, M., Carter, P. H., Khatri, A., Potts, J. T., Jr., and Gardella, T. J. (2001) *Endocrinology 142*, 3068−3074.
12. Shimizu, M., Potts, J. T., and Gardella, T. J. (2000) *J. Biol. Chem. 275*, 21836−21843.
13. Luck, M. D., Carter, P. H., and Gardella, T. J. (1999) *Mol. Endocrinol. 13*, 670−680.
14. Shimizu, N., Guo, J., and Gardella, T. J. (2001) *J. Biol. Chem. 276*, 49003−49012.
15. Roelz, C., Pellegrini, M., and Mierke, D. F. (1999) *Biochemistry 38*, 6397−6405.
16. Houston, M. E., Jr., Gannon, C. L., Kay, C. M., and Hodges, R. S. (1995) *J. Pept. Sci. 1*, 274−282.
17. Houston, M. E., Jr., Campbell, A. P., Lix, B., Kay, C. M., Sykes, B. D., and Hodges, R. S. (1996) *Biochemistry 35*, 10041−10050.
18. Shimizu, N., Petroni, B. D., Khatri, A., and Gardella, T. J. (2003) *Biochemistry 42*, 2282−2290.
19. Braunschweiler, L., and Ernst, R. R. (1983) *J. Magn. Reson. 53*, 521−528.
20. Bax, A., and Davis, D. G. (1985) *J. Magn. Reson. 65*, 355−360.
21. Macura, S., Huang, Y., Suter, D., and Ernst, R. R. (1981) *J. Magn. Reson. 43*, 259−281.
22. Jeener, J., Meier, B. H., Bachmann, P., and Ernst, R. R. (1979) *J. Chem. Phys. 71*, 4546−4553.
23. Piotto, M., Saudek, V., and Sklenar, V. (1992) *J. Biomol. NMR 2*, 661−665.
24. Bodenhausen, G., Vold, R. L., and Vold, R. R. (1980) *J. Magn. Reson. 37*, 93−106.
25. Delaglio, F., Grzesiek, S., Vuister, G. W., Zhu, G., Pfeifer, J., and Bax, A. (1995) *J. Biomol. NMR 6*, 277−293.
26. Goddard, T. D., and Kneller, D. G. (2001) Sparky, NMR Assignment and Integration Software, University of California, San Francisco.
27. Wishart, D. S., Sykes, B. D., and Richards, F. M. (1992) *Biochemistry 31*, 1647−1651.
28. (1994) *Two-Dimensional NMR Spectroscopy: Applications for Chemists and Biochemists*, 2nd ed., John Wiley & Sons, Inc., New York.
29. Wüthrich, K., Billeter, M., and Braun, W. (1983) *J. Mol. Biol. 169*, 949−961.
30. Havel, T. F. (1991) *Prog. Biophys. Mol. Biol. 56*, 43−78.
31. Mierke, D. F., Geyer, A., and Kessler, H. (1994) *Int. J. Pept. Protein Res. 44*, 325−331.
32. Mierke, D. F., Scheek, R. M., and Kessler, H. (1994) *Biopolymers 34*, 559−563.
33. Berendsen, H. J. C., van der Spoel, D., and van Buuren, R. (1995) *Comput. Phys. Commun. 95*, 43−56.
34. van Buuren, A. R., Marrink, S., and Berendsen, H. J. C. (1993) *J. Phys. Chem. 97*, 9206−9216.
35. Pellegrini, M., Bisello, A., Rosenblatt, M., Chorev, M., and Mierke, D. F. (1998) *Biochemistry 37*, 12737−12743.
36. Piserchio, A., Bisello, A., Rosenblatt, M., Chorev, M., and Mierke, D. F. (2000) *Biochemistry 39*, 8153−8160.
37. Mierke, D., and Pellegrini, M. (1999) *Curr. Pharm. Des. 5*, 21−36.
38. Wuthrich, K. (1986) *NMR of Proteins and Nucleic Acids*, John Wiley, New York.
39. Havel, T. F. (1990) *Biopolymers 29*, 1565−1585.
40. Sargent, D. F., and Schwyzer, R. (1986) *Proc. Natl. Acad. Sci. U.S.A. 83*, 5774−5778.
41. Schwyzer, R. (1991) *Biopolymers 31*, 785−792.
42. Schwyzer, R. (1992) *Braz. J. Med. Biol. Res. 25*, 1077−1089.
43. Moroder, L., Romano, R., Guba, W., Mierke, D. F., Kessler, H., Delporte, C., Winand, J., and Christophe, J. (1993) *Biochemistry 32*, 13551−13559.
44. Inooka, H., Ohtaki, T., Kitahara, O., Ikegami, T., Endo, S., Kitada, C., Ogi, K., Onda, H., Fujino, M., and Shirakawa, M. (2001) *Nat. Struct. Biol. 8*, 161−165.
45. Shimizu, M., Shimizu, N., Tsang, J., Petroni, B. D., Khatri, A., and Gardella, T. J. (2002) *Biochemistry 41*, 13244−132.

BI035703I